Available online at www.sciencedirect.com
SCIENCE DIRECT®
International Journal of Thermal Sciences 45 (2006) 335–346
International Journal of Thermal Sciences
www.elsevier.com/locate/ijts

Effect of surface radiation on conjugate natural convection in partially open enclosures

G. Lauriat *, G. Desrayaud

University of Marne-la-Vallée, LETEM, F-77454 Marne-la-Vallée cedex 2, France

Received 19 April 2005; received in revised form 7 July 2005; accepted 12 July 2005
Available online 8 September 2005

Abstract

The heat transfer by natural convection and surface radiation in a two-dimensional vented enclosure in contact with a cold external ambient and a hot internal ambient was studied numerically. Inlet and outlet openings were located at a vertical conducting side wall in contact with hot air. Special attention was given on the modeling of the flow and thermal boundary conditions applied at the side wall. The temperature difference between the two vertical facing sides of the enclosure induces downward buoyancy-driven flow of air within the enclosure and boundary layer flow along the surface immersed into the hot internal ambient. The first part of the study focuses on the conjugate problem of natural convection and wall conduction for various thermal resistances of the cold wall, considered as the main floating parameter through the present study. The effects of surface radiation are discussed in the second part of the paper. The radiative exchanges between the facing walls serve to decrease the difference in the averaged temperatures of the vertical walls. Radiation tends to significantly decrease the temperature of the hot wall while the increase in temperature of the cold wall is less important. The interplay between convection and radiation is discussed and it is shown that radiation contribution in heat transfer dominates for all of the cases investigated.

Keywords: Vented enclosure flows; Surface radiation; Natural convection; Conjugate heat transfer; Numerical heat transfer

1. Introduction

Natural convection in vertical vented enclosure occurs in applications such as cooling of electronic equipment, energy conservation in buildings, double-glass ventilated windows, transformers, nuclear technology and many others fields. While natural convection in closed enclosure has received considerable attention during the past several decades, relatively few studies have been directed at vertically vented enclosures. According to Sefcik et al. [1] the vertical venting designation indicates that the buoyancy-driven flow and heat transfer are restricted by vent openings at the top and bottom boundary walls of the enclosure. Geometrical configurations such as Trombe wall systems used for passive solar heating of buildings, for example, belong to this class of problems. For these cases, the design of vented enclosures involves more geometrical and thermophysical parameters than the classic problem of natural convection in partially open cavities with a fixed thermal contrast between opposing walls. Natural convection in partially open enclosures with a conducting side-wall was numerically studied by Desrayaud and Lauriat [2]. A tall slender cavity having vent openings located at the bottom and top of a vertical sidewall in contact with a hot ambient was considered (Fig. 1). The interaction between the boundary-layer flow along the side of the conducting wall immersed into the internal ambient and the flow within the vented enclosure was examined in detail. For this conjugate problem, the key geometrical parameters which control the buoyancy-driven flow and thermal efficiency of the device are the spacing between the two vertical walls, the widths of inlet and outlet openings and their locations while the buoyancy force depends strongly on the difference in temperature between the hot ambient and the internal surface of the outside wall, and on the thermal resistance of the outside wall.

The main purpose of the present study is the analysis of the coupling of natural convection with radiative exchanges between surfaces, for the same geometry as in [2]. The interaction

* Corresponding author.
E-mail address: lauriat@univ-mlv.fr (G. Lauriat).

1290-0729/$ – see front matter
doi:10.1016/j.ijthermalsci.2005.07.002

Nomenclature

A	enclosure aspect ratio $= H/D$
B	vertical extension of the computational domain. m
C_p	specific heat ..... $J{\cdot}kg^{-1}{\cdot}K^{-1}$
D	width of the vented enclosure ..... m
e	thickness of the glass sheet ..... m
g	gravitational acceleration ..... $m{\cdot}s^{-2}$
G_V	volumetric flow rate ..... $m^3{\cdot}h^{-1}$
h	height of the glass sheet above and below the vent openings ..... m
H	height of the vented enclosure ..... m
k	thermal conductivity ..... $W{\cdot}m^{-1}{\cdot}K^{-1}$
K_e	thermal conductance of the outside wall ..... $W{\cdot}m^{-2}{\cdot}K^{-1}$
l	size of the vent openings ..... m
N_k	thermal conductivity ratio, $= k_{GS}/k_f$
N_r	radiation number, $= \sigma T_h^4/(k_f \Delta T/H)$
P	dimensionless pressure defect, $= p/(\rho_0 g\beta \Delta T H)$
Pr	Prandtl number, $= \nu/\alpha$
q_r	net radiative heat flux density ..... $W{\cdot}m^{-2}$
Q	overall heat flux per unit depth ..... $W{\cdot}m^{-1}$
Q_r	dimensionless net radiative heat flux density, $= q_r/\sigma T_h^4$
Q_V	energy flow rate ..... $W{\cdot}m^{-1}$
Ra_H	Rayleigh number based on the height of the enclosure, $= g\beta(T_h - T_c)H^3/\alpha\nu$
R_e	thermal resistance ..... $m^2{\cdot}K{\cdot}W^{-1}$
T	temperature ..... K
T_0	reference temperature, $= (T_c + T_h)/2$ ..... K
T_h^*	dimensionless hot temperature, $= T_h/\Delta T$
(U, V)	dimensionless velocity components, $= (u, v)/\sqrt{g\beta\Delta T H}$
W	horizontal extension of the computational domain ..... m
(X, Y)	dimensionless coordinates, $= (x, y)/H$

Greek symbols

α	thermal diffusivity ..... $m^2{\cdot}s^{-1}$
β	volumetric coefficient of thermal expansion . K^{-1}
ΔT	temperature difference, $= (T_h - T_c)$ ..... K
ε_i	emissivity of surface i
ρ_0	reference density ..... $kg{\cdot}m^{-3}$
σ	Stefan–Boltzmann constant ..... $W{\cdot}m^{-2}{\cdot}K^{-4}$
θ	dimensionless temperature difference, $= (T - T_h)/(T_h - T_c)$
Θ	dimensionless temperature T/T_h
ν	kinematic viscosity ..... $m^2{\cdot}s^{-1}$

Subscripts

b	bottom
BV	bottom vent
c	cold
f	fluid
GS	glass sheet
h	hot
OW	outside wall
t	top
UV	upper vent

Superscript

$*$	dimensionless quantity

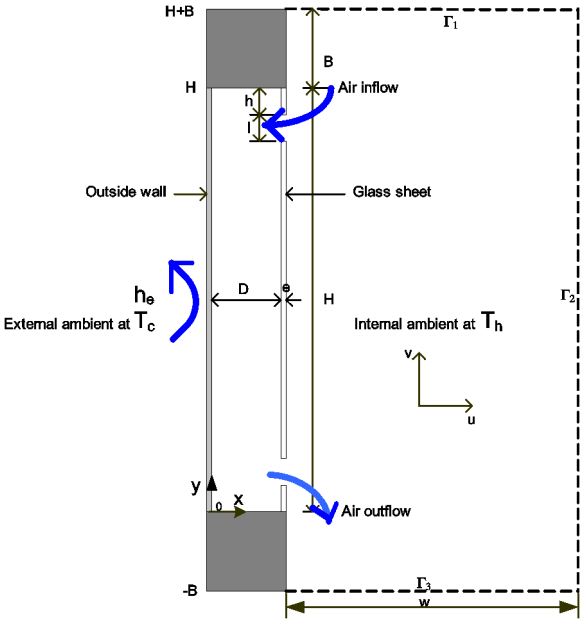

Fig. 1. Geometry of the vented enclosure and computational domain (dashed lines).

of natural convection and radiative transfer in semi-transparent media enclosed in differentially heated cavities has been considered in many papers, as in [3–7], while the effects of surface radiation has, surprisingly, motivated less studies although thermal radiation always exists for air-filled enclosures. The changes in thermal boundary conditions may indeed lead to large effects on the flow structure. To our best knowledge, one of the first studies devoted to this class of problem was presented in a conference paper by Lauriat [8]. Studies published in the archival literature involving multi-mode heat transfer in closed cavities were then very scarce, at least until the recent years [9–16]. It should be emphasized that the influence of surface radiation on air natural convection is one of the most commonly encountered problems at room temperature and, therefore, in the human environment. About fifty percent of heat is transferred by radiation between the glass sheets of an ordinary double-glass window (i.e. without deposited selective film for decreasing long wave radiation exchanges), within the cavities of hollow bricks and breeze-blocks commonly used for building houses in European countries, in living rooms, etc. One of the main reasons which could be invoked for having neglected the interaction of surface radiation with natural convection in

enclosures at room temperature is that it is common to linearize the radiative part of the problem, and then to add convective and radiative contributions through a total heat transfer coefficient or by using a radiation network model [10]. Linearization of radiative terms is of course pertinent, especially when the Boussinesq approximation is invoked. However, the flow equations involving both radiative and convective terms cannot be linearized: as a result, changes in thermal boundary conditions may lead to large changes in the flow characteristics, such as the critical Rayleigh numbers for transition to unsteady flows in a differentially heated cavity [17]. The effects of surface radiation also explain why experiments conducted in air-filled enclosures exhibit large discrepancies with numerical solutions [18] when careful arrangements are not made to eliminate the effects of radiation in the design of an experimental set-up, or when the radiative part is not included in the problem formulation.

The aim of this paper is thus to demonstrate the importance of the effects of surface radiation, through an example of practical application. On account of the number of parameters involved, even for vertically 2D-square or cubic differentially heated enclosures with adiabatic horizontal walls, computations carried out just by successively varying one of the five dimensionless parameters which emerge in the problem formulation (five parameters being the minimum number of parameters) can be useless. That is due to the difficulty in finding a real problem which matches such parametric studies. Therefore, we are reconsidering the practical problem which motivated our previous work [2], i.e. the efficiency of protective glazing used as a thermal barrier to protect glass windows in historic buildings. The results discussed in the present paper add the effects of surface radiation and consider a more general thermal boundary condition at the cold wall, whose temperature distribution depends on an external convective coefficient.

2. Mathematical formulation

It is assumed that the flow is two-dimensional, incompressible, laminar and that the Boussinesq approximation can be applied for a constant property fluid. The schematic of the problem geometry consisting of a vertical vented enclosure of height H, wall spacing D, with the wall of thickness e (called glass sheet in what follows) having bottom and top vent openings of size h, is shown in Fig. 1. Since the flow and heat transfer for a vented enclosure having vents located at a vertical boundary are governed by elliptical, partial differential equations, the solution is sensitive to the assumptions used for modeling inlet and outlet flow conditions. The influence of inlet conditions on natural convection in vertically open channels was discussed in many papers during the past decades but a long-ranging controversy exists regarding the best boundary conditions to be retained [15,19]. Alternative procedures consist in extending the domain of integration to bypass the problem of prescribing boundary conditions at the channel entry and exit. This question was discussed in Desrayaud and Lauriat [2], and it was explained that extension of the computational domain far from the vent openings is basically required for two reasons. First, the shear stresses are not small in the regions close to the openings since the hot fluid does not penetrate axially into the channel. Second, any realistic thermal boundary condition can be applied at the surface of the glass sheet in contact with the internal ambient because the convective heat transfer coefficients may be of the same order of magnitude at both sides of the glass sheet, and vary significantly from the bottom to the top. In addition, for a transient problem in which the external ambient temperature could be lower or higher than internal ambient temperature, one of the vent opening could be either an inlet or an outlet opening according to the sign of the horizontal temperature gradient. Therefore, the computational domain shown in Fig. 1 is closed with three fictitious boundaries(dashed lines Γ_1, Γ_2 and Γ_3 in Fig. 1), open to allow fluid to move in and out. These boundaries have to be located far enough from the vented enclosure in order not to perturb significantly both the flow inside the enclosure and the external flow along the bounding wall.

2.1. Governing equations

With the above assumptions, the equations in the fluid domain are cast in dimensionless form by scaling lengths, velocity, pressure and temperature difference $(T - T_h)$ by H, $\sqrt{g\beta\Delta T H}$, $(\rho_0 g\beta\Delta T H)$ and $\Delta T = (T_h - T_c)$, respectively.

For the coordinate system shown in Fig. 1, the dimensionless governing equations in the flow region consisting in the vented channel and the internal ambient can be written as:

$$\frac{\partial U}{\partial X} + \frac{\partial V}{\partial Y} = 0 \tag{1}$$

$$U\frac{\partial U}{\partial X} + V\frac{\partial U}{\partial Y} = -\frac{\partial P}{\partial X} + \sqrt{\frac{Pr}{Ra_H}}\left(\frac{\partial^2 U}{\partial X^2} + \frac{\partial^2 U}{\partial Y^2}\right) \tag{2}$$

$$U\frac{\partial V}{\partial X} + V\frac{\partial V}{\partial Y} = -\frac{\partial P}{\partial Y} + \sqrt{\frac{Pr}{Ra_H}}\left(\frac{\partial^2 V}{\partial X^2} + \frac{\partial^2 V}{\partial Y^2}\right) + \left(\theta + \frac{1}{2}\right) \tag{3}$$

$$\frac{\partial U\theta}{\partial X} + \frac{\partial V\theta}{\partial Y} = \frac{1}{\sqrt{Pr\,Ra_H}}\left(\frac{\partial^2 \theta}{\partial X^2} + \frac{\partial^2 \theta}{\partial Y^2}\right) \tag{4}$$

In the glass sheet, the dimensionless heat equation is

$$\left(\frac{\partial^2 \theta_{GS}}{\partial X^2} + \frac{\partial^2 \theta_{GS}}{\partial Y^2}\right) = 0 \tag{5}$$

2.2. Surface radiation calculations

When radiative interchanges among surfaces are accounted for, the thermal boundary conditions at the solid walls must include the contribution of the net radiative flux. For the problem considered here, the four surfaces bounding the vented airspace and the surface in contact with the internal ambient are subjected to surface radiation.

By assuming that all of the solid–fluid interfaces are grey, diffusively emitting and diffusively reflecting surfaces, the dimensionless temperature for the radiative part of the problem formulation, $\Theta_i(r_i) = T/T_h$, and dimensionless net radiative fluxes, $Q_{r,i}(r_i) = q_{r,i}(r_i)/\sigma T_h^4$, can be related by a set of four

linear Fredholm integral equations of the second kind [20]. In these equations r_i is the space coordinate for surface S_i ($i = 1, \ldots, 4$) of the vented enclosure. This formulation, not taking to recourse to radiosity, is suitable to the present configuration

$$\Theta_i^4(r_i) - \frac{Q_{r,i}(r_i)}{\varepsilon_i} = \sum_{j=1}^{4} \int_{S_j} \Theta_j^4(r_j) K(r_i, r_j)\, \mathrm{d}S_j - \sum_{j=1}^{4} \int_{S_j} \frac{1-\varepsilon_j}{\varepsilon_j} Q_{r,j}(r_j) K(r_i, r_j)\, \mathrm{d}S_j, \quad 1 \leqslant i \leqslant 4 \tag{6}$$

where $K(r_i, r_j) = \cos(\theta_i)\cos(\theta_j)/\pi r_{i,j}^2$ is the kernel of the integral equations [20]. Each of these four equations contains eight temperature and heat flux functions. Therefore, four of these must be prescribed. Since the four facing surfaces involve heat flux boundary conditions, it could be assumed that an initial guess for $\Theta_i^4(r_i)$ is given by the solution of the energy equation.

The radiation exchanges between the internal surface of the glass sheet and the internal ambient do not require to solve a linear system of integral equations because the internal ambient is considered as an infinite space at blackbody temperature T_h. Thus, the net radiative flux along the surface of the glass sheet is explicitly written in the following dimensionless form

$$Q_{r,i}(Y) = \varepsilon_i \left(\Theta_i^4(Y) - 1\right) \tag{7}$$

Since $\Theta_i = T/T_h = \frac{\Delta T}{T_h}\theta_i + 1$, the dimensionless temperature difference is introduced as an additional parameter when surface radiation is accounted for.

2.3. Boundary conditions

From Fig. 1 which shows the general layout of the problem, the boundary conditions are:

- Internal surfaces of the enclosure

Non-slip conditions and energy balances between convection, conduction and radiation lead to

(1) Along the adiabatic horizontal end walls of the enclosure

$$\nabla\theta.\vec{n} = N_r Q_r(X)$$
$$U = V = 0$$
$$\text{at } Y = 0, 1 \text{ and } 0 \leqslant X \leqslant D^* \tag{8}$$

where $\vec{n}$ is the outward normal to the surface considered.

(2) Along the vertical outside wall

$$\frac{\partial\theta}{\partial X} = K_e^*(\theta + 1) - N_r Q_r(Y)$$
$$U = V = 0$$
$$\text{at} \quad X = 0 \text{ and } 0 \leqslant Y \leqslant 1 \tag{9}$$

where K_e^* is the dimensionless thermal conductance of the outside wall including conduction through the wall and convection with the external cold air ($K_e^* = K_e H/k_f$ where K_e is the dimensional thermal conductance). The contributions of conduction and external convection in the K_e-values are discussed in the result section.

(3) Along the surface of the glass sheet

$$\begin{cases} \frac{\partial\theta}{\partial X} = N_k \frac{\partial\theta_{GS}}{\partial X} + N_r Q_r(Y) \\ \theta = \theta_{GS} \end{cases} \tag{10}$$
$$U = V = 0 \tag{11}$$

at $X = D^*$ and $0 \leqslant Y \leqslant Y_1$; $Y_2 \leqslant Y \leqslant Y_3$; $Y_4 \leqslant Y \leqslant 1$ where $Y_1 = h^*$, $Y_2 = h^* + l^*$, $Y_3 = 1 - (h^* + l^*)$ and $Y_4 = 1 - h^*$.

In Eqs. (8)–(10), Q_r are implicitly given by the system of Eq. (6).

(4) Surface in contact with the internal ambient

$$\begin{cases} \frac{\partial\theta}{\partial X} = N_k \frac{\partial\theta_{GS}}{\partial X} - \varepsilon N_r \left(\left(\frac{\theta}{T_h^*} + 1\right)^4 - 1\right) \\ \theta = \theta_{GS} \end{cases} \tag{12}$$
$$U = V = 0 \tag{13}$$

at $X = D^* + e^*$ and $0 \leqslant Y \leqslant Y_1$; $Y_2 \leqslant Y \leqslant Y_3$; $Y_4 \leqslant Y \leqslant 1$. and

$$\frac{\partial\theta}{\partial X} + \varepsilon N_r \left(\left(\frac{\theta}{T_h^*} + 1\right)^4 - 1\right) = 0 \tag{14}$$
$$U = V = 0 \tag{15}$$

at $X = D^* + e^*$ and $-B^* \leqslant Y \leqslant 0$; $1 \leqslant Y \leqslant 1 + B^*$

$$U = V = 0 \tag{16}$$

The temperature and flow conditions applied at the boundaries of the computational domain indicated as Γ_1, Γ_2 and Γ_3 in Fig. 1 are

- Top boundary Γ_1:

$$\frac{\partial\theta}{\partial Y} = 0; \quad U = V = 0 \quad \text{at } Y = 1 + B^* \ \forall X \geqslant D^* + e^* \tag{17}$$

- Right-hand side boundary Γ_2:

$$\theta = 0.5; \quad U = 0; \quad \frac{\partial V}{\partial X} = 0 \quad \text{at } X = D^* + e^* + W^* \text{ and } -B^* \leqslant Y \leqslant 1 + B^* \tag{18}$$

- Bottom boundary Γ_3

$$\frac{\partial\theta}{\partial Y} = 0 \quad \text{if } V \leqslant 0 \text{ or } \theta = 0.5 \text{ if } V > 0$$
$$U = \frac{\partial V}{\partial Y} = 0 \quad \text{at } Y = -B^* \ \forall X \geqslant D^* + e^* \tag{19}$$

In the above set of equations it can be seen that the geometry of the problem is characterized by four dimensionless lengths: the dimensionless width of the enclosure, D^* or, equivalently, the height-to-width aspect ratio $A = H/D = 1/D^*$, the dimensionless thickness of the glass sheet, e^*, the dimensionless height of

the parts above and below the openings, h^*, the dimensionless width of the openings l^*. The dimensionless lengths B^* and W^* are only related to the size of the external computational domain, and should be taken to be sufficiently large to have a negligible influence on the flow field within the enclosure (i.e. $B^* \approx 0.25$ and $W^* \geqslant 1$).

The relevant dimensionless thermophysical parameters for the present conjugate problem accounting for convection, conduction and radiation are the Rayleigh number based on the height of the vented enclosure, Ra_H, the Prandtl number, Pr, the thermal conductivity ratio, N_k, the dimensionless conductance of the outside wall, K_e^*, the radiation number, N_r or the Planck number $Pl = 1/N_r$, the dimensionless hot temperature, T_h^*, and the wall emissivities, ε_i . In the present work, we have chosen to conduct the analysis with $\varepsilon_i = \varepsilon$ in order not to increase the number of parameters. The differences in surfaces emissivities for the practical application under consideration are indeed rather small. The effect of surface radiation thus adds three dimensionless parameters in the problem formulation (N_r, T_h^* and ε) which depends upon 4 geometrical parameters and 7 flow and thermal parameters.

3. Solution procedure and code validation

The transport equations were discretized on structured control volumes using a second-order QUICK-type scheme for the convection terms and by employing the SIMPLER pressure correction algorithm. The momentum and energy equations were cast in transient form and the time-integration was performed using a false-transient scheme based on an ADI method with a much larger time step for the energy equation than for the momentum equation. When the time steps are not very small, inner iterations are required to account for the non-linearity of the equations. In the present study, under-relaxation parameters were introduced for velocities and temperature to control the advancement of the solution field until a steady state was obtained. The suitable values of the relaxation factors were found by experience.

The system of integral equations for the net radiative flux along the facing surfaces of the vented enclosure were transformed into a linear system of algebraic equations by breaking up the surfaces into NS isothermal subsurfaces, the temperature of which being evaluated from the temperature distribution calculated at the previous time step of the numerical procedure used for integrating the conservation equations. The integral terms in the right-hand side of Eq. (6) were represented by summations using the Simpson rule and, the number NS of subsurfaces was defined either by the mesh used for integrating the flow equations or by clustering few mesh surfaces in order to reduce the size of the matrix systems. The dimensionless net radiative flux, $Q_{r,j}$, at subsurface $\mathrm{d}S_j$ located on the surface S_j of the vented enclosures was thus obtained by solving the system of algebraic equations

$$\sum_{j=1}^{NS}\left[\frac{\delta_{ij}}{\varepsilon_j} - F_{ij}\frac{1-\varepsilon_j}{\varepsilon_j}\right]Q_{r,j} = \sum_{j=1}^{NS} F_{ij}\left(\Theta_i^4 - \Theta_j^4\right)$$
$$\text{for } 1 \leqslant i \leqslant NS \tag{20}$$

Table 1
Comparison of convective (Nu_c) and total (Nu_t) mean Nusselt numbers along the hot wall for $Ra_H = 6.21 \times 10^4$, $N_r = 6.36$ and $T_0/T_h = 0.866$ (Nakamura et al. [9])

ε_H	ε_p	[9]		Present	
		Nu_c	Nu_t	Nu_c	Nu_t
0.03	0.03	1.33	1.39	1.31	1.36
1	0.33	1.24	1.47	1.23	1.44
1	1	1.09	3.89	1.08	3.84

In Eq. (20), $\delta_{ij} = 0$ if $i \neq j$ and $\delta_{ij} = 1$ if $i = j$. F_{ij} is the view factor between two subsurfaces dS_i and $\mathrm{d}S_j$. For the two-dimensional geometry considered here, the Hottel crossed-string method allows exact evaluations of the view factors. The convergence criteria for steady state included checks on the overall mass and energy balance for the vented enclosure, and relative changes between consecutive iterations. Both the mass and energy balances were found satisfactory within less than 0.7% in the entire flow regime investigated.

The numerical code was also extensively validated against benchmark problems for pure natural convection and closely related problems to check its validity for solving conjugate natural convection. Comparison results such those presented in Desrayaud and Lauriat [2] are omitted here for brevity. The grid tests reported in [2] have shown that a 100×200 grid resolution (streamwise $\times$ cross-stream directions) yielded a good compromise between accuracy and computational time.

When including surface radiation for cavities with heat flux boundary conditions at the walls, it is well established that the general trends are slight reductions of the temperature gradient normal to the walls and of the maximal flow velocities, especially at high Rayleigh numbers. These trends were observed in the present study and, consequently, the previously reported grid tests made for pure natural convection can be viewed as still valid.

A comparison of the present results and those of Nakamura et al. [9] for natural convection—surface radiation interaction in an air-filled enclosure of aspect ratio $A = 5$ with a partition wall located at cavity midplane is shown in Table 1. The total and radiative Nusselt numbers for different hot wall emissivities (ε_h) are for a partionned cavity having an emissivity of the partition ε_p on both sides. As it can be seen, the agreement between the solutions is fairly good.

4. Results and discussion

The ranges of the 15 dimensional parameters used in the present work are listed in Table 2 while the ranges of the 11 dimensionless numbers are reported in Table 3. The dimensional parameters can be classified into three general groups: geometric characteristics, material properties and external effects, as it is shown in Table 2. The four basic dimensions (mass, length, time and temperature) being used, the Buckingham π-theorem indicates that the number of independent dimensionless parameters cannot be larger than 11. In other words, a Nusselt number correlation cannot be derived in terms of these 11 dimensionless numbers. Therefore, it has been decided to relate

Table 2
Ranges of dimensional parameters

Parameter	Value	Units
Geometric characteristics		
D	0.04	m
e	0.005	m
h	0.02	m
H	4.0	m
l	0.04	m
Material properties		
C_p	1008	$\mathrm{J\cdot kg^{-1}\cdot K^{-1}}$
k_f	0.025	$\mathrm{W\cdot m^{-1}\cdot K^{-1}}$
k_{GS}	1.0	$\mathrm{W\cdot m^{-1}\cdot K^{-1}}$
μ	1.76×10^{-5}	$\mathrm{kg\cdot m^{-1}\cdot s^{-1}}$
ρ	1.265	$\mathrm{kg\cdot m^{-3}}$
ε	$0\leqslant\varepsilon\leqslant0.95$	
External effects		
K_e	$2.28\leqslant K_e\leqslant60$	$\mathrm{W\cdot m^{-2}\cdot K^{-1}}$
T_c	$268\leqslant T_c\leqslant278$	K
T_h	288	K
β	$3.5\times10^{-3}\leqslant\beta\leqslant3.6\times10^{-3}$	$\mathrm{K^{-1}}$

Table 3
Ranges of dimensionless parameters

Parameter	Value
Geometry	
D^*	0.01
e^*	0.00125
h^*	0.005
H^*	1
l^*	0.01
Flow and heat transfer parameters	
K_e^*	$3.2\times10^2\leqslant K_e^*\leqslant9.6\times10^3$
N_r	$3.12\times10^3\leqslant N_r\leqslant6.24\times10^3$
N_k	40
Pr	0.71
Ra_H	$8.1\times10^{10}\leqslant Ra_H\leqslant16.6\times10^{10}$
ε	$0\leqslant\varepsilon\leqslant0.95$
T_h^*	$14.4\leqslant T_h^*\leqslant28.8$

the present study to a specific application, namely a device used to prevent condensation of humid air on stained-glass windows in historic buildings [2]. Obviously, another specific problem such as double glass naturally ventilated window [21] could be also selected to highlight the effects of radiation at room temperature. However, to cast the governing equations in dimensionless form is still meaningful because the values of the dimensionless parameters indicate the order of magnitude of the most important effects. For examples, values of Ra_H tell us how is the expected flow régime and, comparisons between K_e^* and N_r in Eq. (9) give the relative importance of conduction through the outside wall and surface radiation.

4.1. Dimensional parameters

There are a large number of model geometrical parameters, thermal conditions, and so on, that describe the vented enclosure. Therefore, it is necessary to be selective. The dimensions of the enclosure considered here and the physical parameters kept constant in the process of the present study are reported in Table 2.

All the computations discussed in the present work were done for air ($Pr = 0.71$), assuming it to be a radiatively transparent fluid. In addition, the geometric characteristics of the vented enclosure are fixed. The height is taken to be $H = 4$ m while the spacing is $D = 0.04$ m. These dimensions are based on experimental studies reported in the literature [22]. The aspect ratio $A = H/D$ is thus very high, typical also of what is found for double glass windows. The sizes of the two vents were $l = 0.04$ m and their locations were at $h = 0.02$ m from the top and bottom end surfaces. The choice $l = D$ and $h \approx D/2$ results from previous computations conducted for a similar geometry by neglecting surface radiation. These computations have shown that $l = D$ is almost the optimal size of the openings to have an efficient convective heating of the inner glass sheet [2]. Therefore, these four geometrical parameters are considered here not to have significant effects on the conclusions about surface radiation effects which could be drawn for similar geometries. Since we are considering air as a Boussinesq fluid with a reference temperature varying in the range $278\ \mathrm{K}\leqslant T_0\leqslant283\ \mathrm{K}$, it may be assumed that the thermophysical properties, except the coefficient of volumetric thermal expansion, keep their values at 280 K. Therefore, the only large change in material properties is that for the emissivity of the walls (Table 2).

The heat losses through the outside wall are accounted for by an overall heat transfer coefficient, K_e, included in the external effects described in Table 2. The variations of K_e are in a quite large range because it depends on the thermal conductance of the wall and on the outside heat transfer coefficient. Let us consider now these two contributions to K_e. The range for wall thermal resistance is taken to be $0.005\ \mathrm{K\cdot m^2\cdot W^{-1}}\leqslant R_e\leqslant 0.34\ \mathrm{K\cdot m^2\cdot W^{-1}}$ because the typical outside walls used in practice are windows made of a single glass sheet, a double, ordinary glass sheets or a double glass sheets having selective radiation properties due to deposited film on one of the glass sheets. These thermal resistances comply with the requirements outlined in ASHRAE [23] which gives also the outside heat transfer coefficient as a function of the wind speed V by the equation $h_e = 10 + 4.1V$ $[\mathrm{W\cdot m^2\cdot K^{-1}}]$. The range of wind speed considered is $0\leqslant V\leqslant10\ \mathrm{m\cdot s^{-1}}$. Therefore, the overall wall conductance varies between $K_e\approx2.0$ and $K_e\approx60\ \mathrm{W\cdot m^{-2}\cdot K^{-1}}$. For K_e larger than $60\ \mathrm{W\cdot m^{-2}\cdot K^{-1}}$, the outside wall surface can be assumed at a uniform temperature close to T_c. The hot ambient temperature $T_h = 288$ K is chosen appropriate for inside temperature of historic buildings. The range for external temperature T_c is typical for winter conditions at which condensation of humid air are observed.

4.2. Dimensionless parameters

When surface radiation is taken into account with all the surfaces having the same emissivity, three additional dimensionless parameters are introduced when adimensionalizing the set

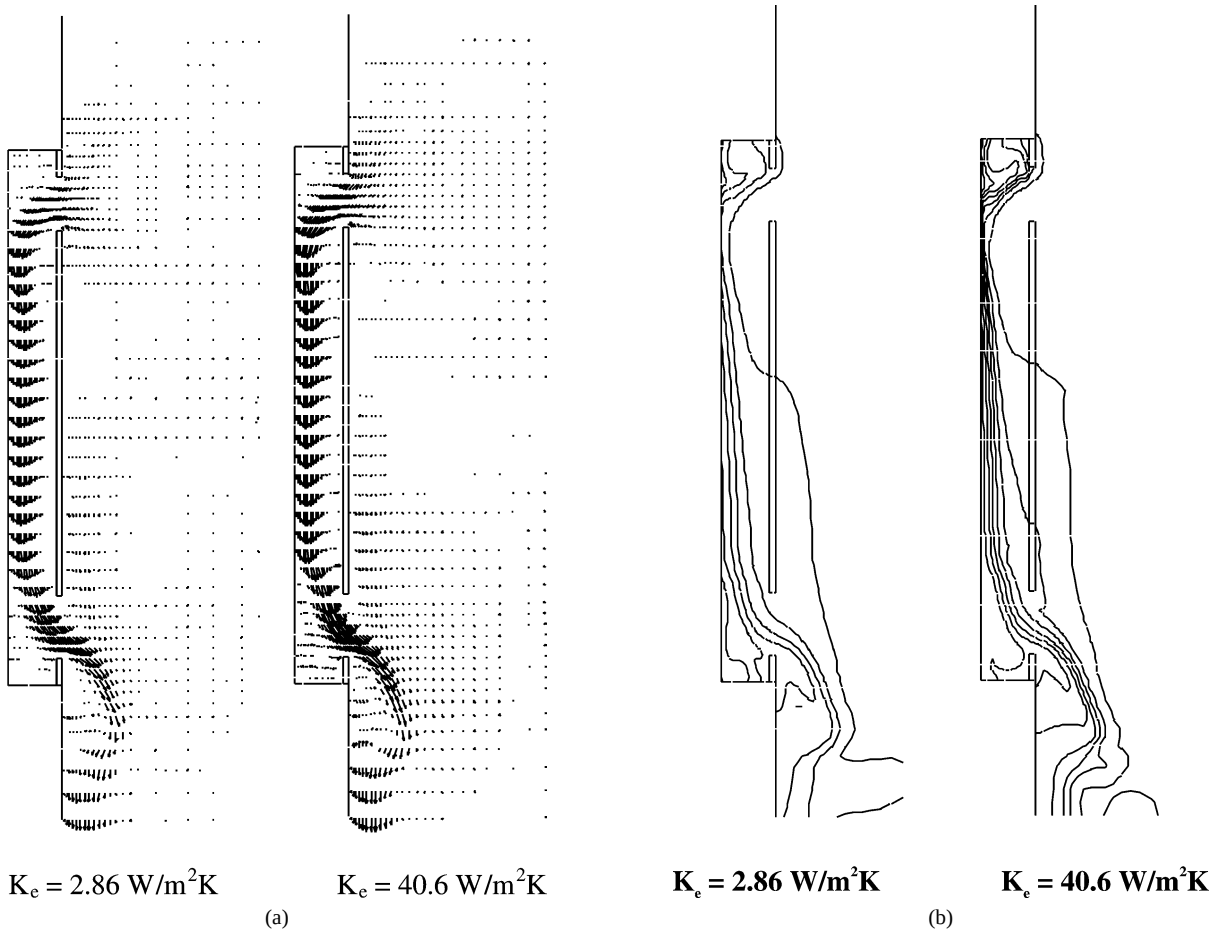

Fig. 2. Velocity vectors (a) and temperature fields (b) within the vented enclosures and along the glass sheet for different conductances K_e of the outside wall (pure natural convection, $\varepsilon_i = 0$).

of governing equations, i.e. the emissivity of the facing walls, ε, the radiation parameter, N_r, and the dimensionless hot temperature, T_h^*. In the present study, the variations in N_r are only due to variations in the temperature difference, ΔT. Therefore, a narrow range of N_r-variations is reported in Table 3. The introduction of a scale for the radiative flux density as σT_h^4 yields the third parameter.

It is to be noted here that the high Rayleigh number reported in Table 3 is based on the maximum temperature difference, i.e. the temperature difference $\Delta T = T_h - T_c$ between the internal and external ambient. From a physical point of view, the relevant Rayleigh number should be based on the temperature difference between the average temperatures of the two vertical facing surfaces of the vented enclosure. In what follows, this relevant Ra_H will be termed as effective Rayleigh number (Ra_{eff}). Nevertheless, the highest values of Ra_H indicate that the flow régime could exhibit a periodic behaviour (with low frequency oscillations) for pure natural convection and large thermal conductance of the external wall.

4.3. Contributions by convection and radiation

In order to isolate the role of surface radiation, results have been obtained first without surface radiation accounted for. Second, the flow characteristics and heat transfer rates are discussed when surface radiation is included. Comparisons with the results of the first stage reveal relative contributions of natural convection and surface radiation to heat transfer.

4.3.1. Isolating the role of surface radiation

We consider first the effect of the thermal conductance of the outside wall while keeping constant all of the other quantities: the external and internal ambient temperatures are $T_c = 0\,^\circ\text{C}$ and $T_h = 15\,^\circ\text{C}$, respectively. Fig. 2 shows the velocity and temperature fields within the vented enclosure and in the near-field from the glass-sheet for the lowest and highest values of thermal conductance considered in the present study. Note that these plots are not drawn to scale in order to make possible plots over the whole extent of the slender enclosure. It can be observed that a jet of hot fluid penetrates into the enclosure through the upper opening with an almost flat horizontal velocity profile, turns right-angled and then proceeds downstream. The enclosure simulates two isolated vertical plates with a well defined thermal boundary layer along the cold outside wall on account of the high Rayleigh numbers considered (Fig. 2(a)). Over most of the height, the flow characteristics are thus similar to those for natural convective flow between vertical parallel plates heated asymmetrically. The flow can be considered as in the single-plate regime for these various values of K_e (Sparrow and Azevedo [24]). When the primary inlet flow approaches

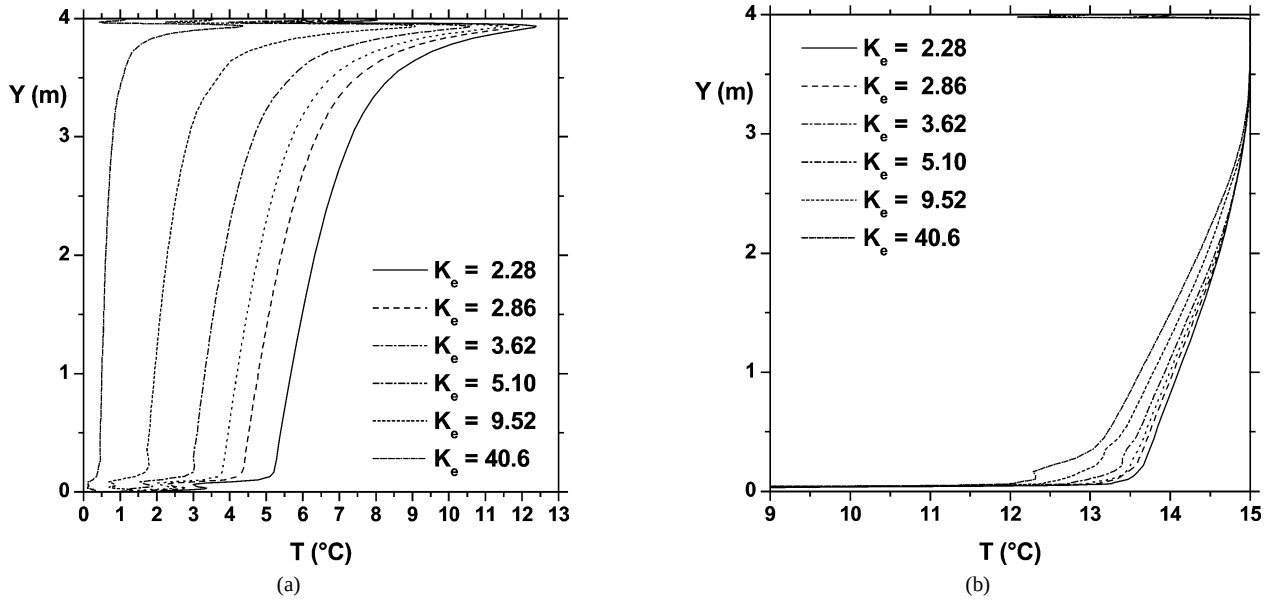

Fig. 3. Vertical temperature profiles along the vertical facing surfaces for different conductances K_e [W·m^{-2}·K^{-1}] of the outside wall (pure natural convection, $\varepsilon_i = 0$). (a) outside wall; (b) glass sheet.

the bottom of the enclosure, the thermal boundary layer meets the glass sheet before turning towards the outlet opening with a mixing-cup temperature decreasing as K_e increases. These observations mean that there is a progressive increase in convection heat transfer along the outside wall, as evidenced by the isothermal patterns plotted in Fig. 2(b). In the present example, the convection heat transfer increases twofold in the range of K_e investigated. The maximum in downward velocity occurs just below the top opening because the fluid in the entrance region is almost at the internal temperature over most of the enclosure width. The thicknesses of the dynamical and thermal boundary layers increase when the fluid proceeds downstream. Therefore, the maximum velocities decrease as the flow spreads towards the glass sheet since the flow rate through any horizontal section is constant (here is the main difference between a channel flow and a flow along a single plate). The velocity fields show quiescent regions at the top and bottom caused by the solid parts above and below the openings. The extension of these regions are almost independent of the Rayleigh number, even for a much larger range of Ra_H than that considered in the present study [2]. On account of the small differences in the flow structure at the upper part of the enclosure, the glass sheet is at almost uniform temperature over the height upper half, whatever the value of K_e is. Since the temperature of the glass sheet is lower than that of the internal ambient, a natural convection flow develops along its internal side too. Thus, the thermal equilibrium of the glass sheet is determined from a conjugate problem: natural convection on its two sides and heat conduction through it. Fig. 2(b) shows that the main thermal influences of K_e on the temperature distribution along the glass sheet are predicted at the bottom part due to an increased cooling by the flow of cold air when proceeding towards the outlet. Obviously, the flow rate of the boundary layer flow along the internal surface of the glass sheet (i.e. for $x > D + e$) depends upon the temperature difference between the glass sheet and the internal ambient, and thus on K_e.

Fig. 3 shows the temperature distributions along the two vertical facing surfaces for various values of K_e. As previously mentioned, the impact of the inlet jet of hot air at the outside wall surface and the weak recirculating flow at the top region of the enclosure lead to a sharp increase in the surface temperatures, except for the highest K_e-value at which the local heat transfer coefficient resulting from the inlet jet is much lower than K_e. The surface temperature decreases then monotonously in the downward direction with a vertical temperature gradient all the more small since K_e is large. For $K_e = 40.6$ W·m^{-2}·K^{-1}, the surface temperature profile at the outside wall reveals, as expected, that the height averaged temperature is close to the external ambient temperature. Other computations predicted that the external ambient temperature was almost recovered over more than 95% of the height for $K_e \approx 60$ W·m^{-2}·K^{-1}. The temperature distribution along the glass-sheet is much less influenced by K_e. The explanation is found in the weak change in the flow structure within the vented enclosure due to the small variations in effective Rayleigh number in the range of K_e investigated. It should be pointed out that the temperature profiles in the region adjacent to the bottom and top horizontal walls of the enclosure indicate that the fluid is almost isothermal, as previously discussed and shown in Fig. 2(b). However, enlargement of these profiles at $y = 0$, H display clearly that the adiabatic boundary condition is met. Finally, Fig. 4 shows the effect of K_e on the height averaged temperatures of the two facing vertical surfaces. The small changes in $\overline{T}_{GS}$ and the large changes in $\overline{T}_{OW}$ are evidenced. Therefore, the increases in the effective Rayleigh number based on $\Delta T_{eff} = \overline{T}_{GS} - \overline{T}_{OW}$ are mostly due the decreases in $\overline{T}_{OW}$ which matches almost the mean temperature $T_0 = (T_c + T_h)/2$ for the lowest K_e-value and the external temperature, T_c, at the highest K_e-value (Fig. 4).

Table 4
Heat fluxes at the outside wall (Q_{OW}), glass sheet (Q_{GS}), enthalpy fluxes through the upper (Q_{UV}) and bottom opening vents (Q_{BV}), volumetric flow rate (G_V) and effective temperature difference. Surface radiation neglected. The K_e-values match various types of outside wall and external heat transfer coefficient (see Section 4.1)

K_e [W·m^{-2}·K^{-1}]	Q_{OW} [W·m^{-1}]	Q_{GS} [W·m^{-1}]	Q_{UV} [W·m^{-1}]	Q_{BV} [W·m^{-1}]	G_V [m^3·h^{-1}]	ΔT_{eff} [°C]
2.28	60.6	−2.7	−86.3	28.4	32.8	7.63
2.86	67.0	−2.8	−89.1	25.3	33.9	8.29
3.62	74.1	−3.1	−91.8	20.9	34.9	8.91
5.10	84.2	−3.5	−96.3	15.7	36.7	10.05
9.52	97.6	−4.0	−100.3	7.2	38.2	11.62
40.6	115.3	−4.8	−105.7	−4.4	42.5	13.44

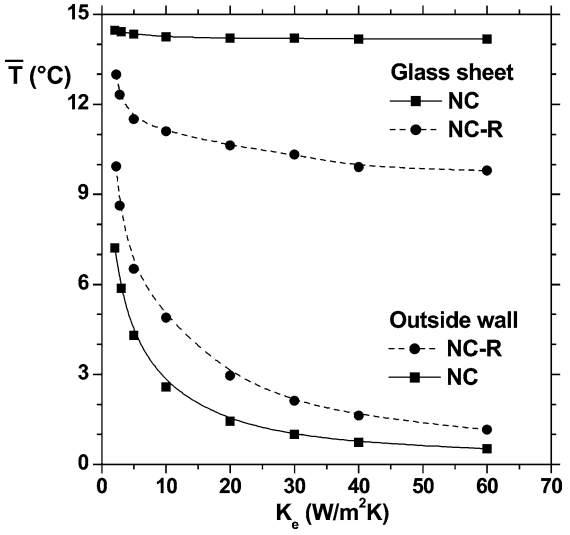

Fig. 4. Variation of the average temperatures of the vertical facing surfaces versus the conductance K_e of the outside wall (NC: pure natural convection ($\varepsilon_i = 0$), NC-R: surface radiation accounted for ($\varepsilon_i = 0.95$)).

Table 4 shows the effects of K_e on the overall heat fluxes Q_{OW} and Q_{GS} at the facing surfaces, the energy flow rate through the top and bottom openings, Q_{UV} and Q_{BV} respectively, the mass flow rate G_V through the inlet vent (or through any horizontal cross-section within the enclosure) and, on the effective temperature difference ΔT_{eff}. Let us first define the quantities reported in Tables 4–6.

The overall heat fluxes at the facing surfaces are obtained as:

$$Q_{OW} = -k_f \int_0^H \left.\frac{\partial T}{\partial x}\right|_0 \mathrm{d}y + \int_0^H \big(R(y) - E(y)\big)_{OW}\,\mathrm{d}y \tag{21}$$

$$Q_{GS} = -k_f \left[\int_0^{y_1} \left.\frac{\partial T}{\partial x}\right|_D \mathrm{d}y + \int_{y_2}^{y_3} \left.\frac{\partial T}{\partial x}\right|_D \mathrm{d}y + \int_{y_4}^{H} \left.\frac{\partial T}{\partial x}\right|_D \mathrm{d}y\right] + \int_0^H \big(R(y) - E(y)\big)_{GS}\,\mathrm{d}y \tag{22}$$

where subscripts OW and GS stand for the outside wall and glass sheet, respectively. $R(y)$ and $E(y)$ are the radiosity and incident radiation flux [20]. The integral terms involving $(R(y) - E(y))$ in Eqs. (21)–(22) are set to zero when surface radiation is neglected.

The energy flow rate and volumetric flow rate through the openings are calculated from

$$\begin{cases} Q_V = \int_l \left[\rho C_p u(D, y)(T - T_0) - k_f \frac{\partial T}{\partial x}|_D\right] \mathrm{d}y \\ G_V = \int_l u(D, y)\,\mathrm{d}y \end{cases} \tag{23}$$

where l stands for the opening widths ($l = y_2 - y_1$ or $y_4 - y_3$). The flow structures shown in Fig. 2 tell us that the dominant term in Q_V is the transport term, whatever K_e is.

Energy conservation requires that

$$Q_{OW} + Q_{GS} + Q_{UV} + Q_{BV} = 0 \tag{24}$$

where subscripts UV and BV stand for the upper and bottom opening vent, respectively.

Table 4 shows first that the heat flux at the outside wall is almost doubled when K_e increases from 2.28 W·m^{-2}·K^{-1} to 40.6 W·m^{-2}·K^{-1} while the heat flux transferred at the glass sheet keeps a comparatively low value. A negative sign in Q_{GS} means that heat is transferred by conduction through the glass sheet. It should be recalled here that the lowest K_e-value is for a outside wall made of a selective, double-glass window and a zero wind speed while the highest value is for a single glass window and a wind speed $V = 10$ m·s^{-1}. Most of the energy flow rate through the upper opening is thus transferred at the outside surface and the remaining heat is flowing through the bottom opening, except for $K_e = 40.6$ W·m^{-2}·K^{-1} for which the negative sign means that the mixing-cup temperature of the exit fluid is below the mean fluid temperature.

4.3.2. Effects of surface radiation

When surface radiation effects are accounted for, plots of velocity and temperature fields are presented in Fig. 5 using the same scales as in Fig. 2. The effects of radiation can be summarized as follows:

- Small influences on the flow rate G_V within the enclosure but noticeable decreases in the maximum vertical velocities over most of the enclosure height because the boundary layer structure disappears, especially at low K_e-values where the downwards flow resembles a symmetrically cooled channel flow. Such a change occurs because of a large radiative cooling of the glass sheet compensated by convective heating at both sides. It can be noted that surface radiation produces small decreases in G_V for the lowest K_e value while an opposite trend is predicted when the conductance of the outside wall increases. To summarize, the most

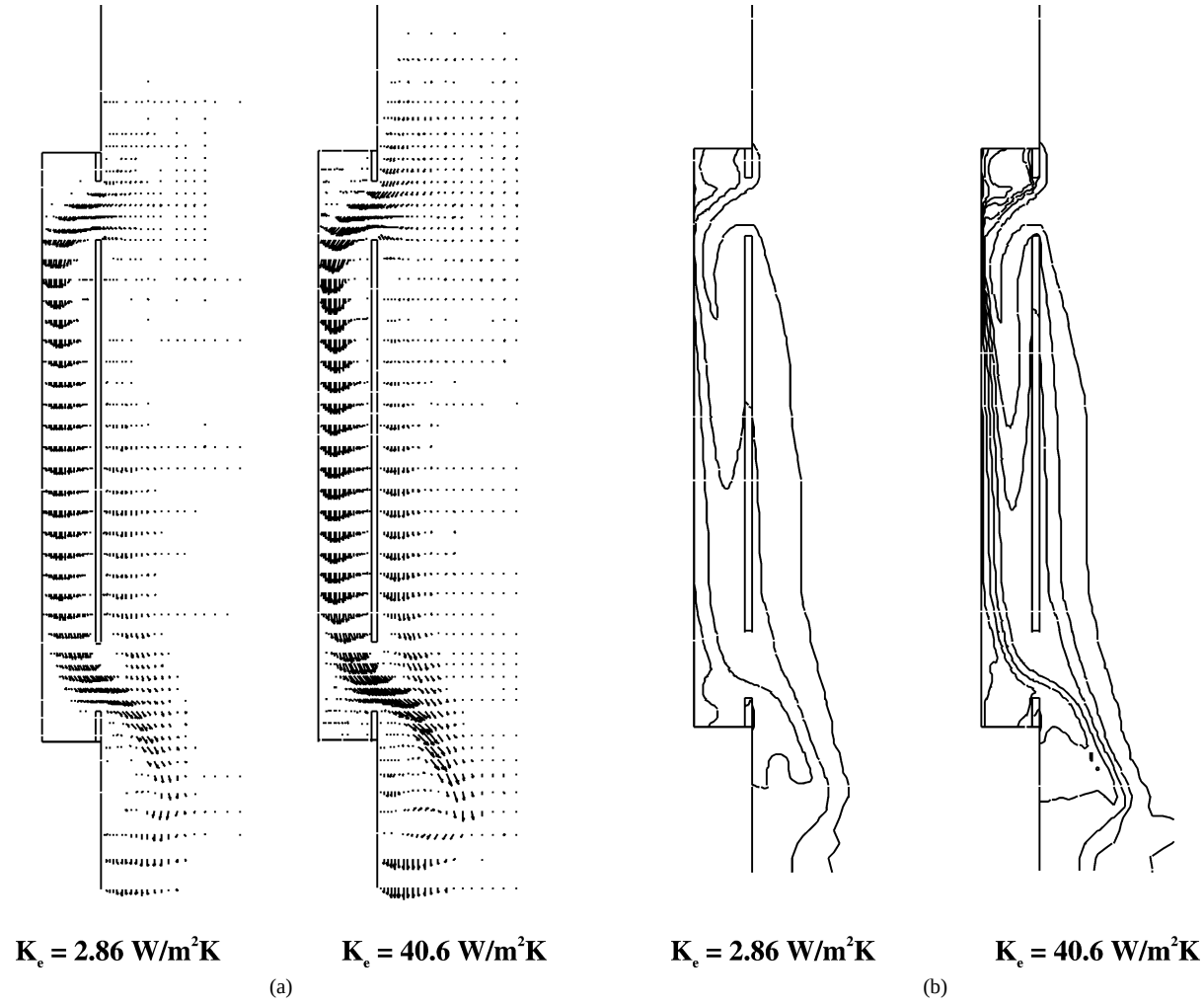

Fig. 5. Velocity vectors (a) and temperature fields (b) within the vented enclosures and along the glass sheet for different conductances K_e of the outside wall with surface radiation ($\varepsilon_i = 0.95$).

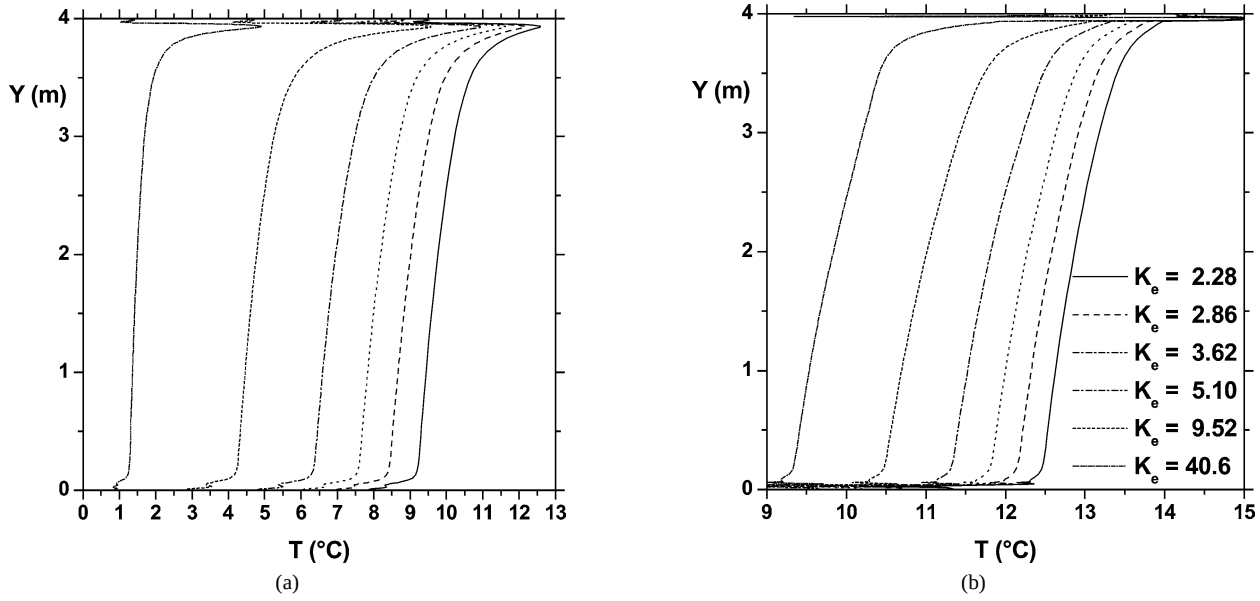

Fig. 6. Vertical temperature profiles along the vertical facing surfaces for different conductances K_e [$\mathrm{W{\cdot}m^{-2}{\cdot}K^{-1}}$] of the outside wall with surface radiation accounted for ($\varepsilon_i = 0.95$). (a) outside wall; (b) glass sheet.

Table 5
Combined convective and radiative heat fluxes at the outside wall (Q_{OW}), glass sheet (Q_{GS}), enthalpy fluxes through the upper (Q_{UV}) and bottom opening vents (Q_{BV}) and volumetric flow rate (G_V) and effective temperature difference

K_e [W·m^{-2}·K^{-1}]	Q_{OW} [W·m^{-1}]	Q_{GS} [W·m^{-1}]	Q_{UV} [W·m^{-1}]	Q_{BV} [W·m^{-1}]	G_V [m^3·h^{-1}]	ΔT_{eff} [°C]
2.28	91.4 $R_{OW} = 59.0$	−54.1 $R_{GS} = -58.3$	−81.4	43.6	30.1	3.27
2.86	106.3 $R_{OW} = 66.8$	−61.6 $R_{GS} = -66.1$	−87.0	42.0	33.5	3.69
3.62	122.9 $R_{OW} = 77.1$	−69.7 $R_{GS} = -76.2$	−92.7	39.6	35.3	4.25
5.10	146.9 $R_{OW} = 91.0$	−81.8 $R_{GS} = -89.9$	−100.4	34.8	38.1	5.00
9.52	189.9 $R_{OW} = 115.2$	−107.0 $R_{GS} = -114.0$	−109.1	21.0	41.4	6.28
40.6	260.8 $R_{OW} = 152.2$	−135.8 $R_{GS} = -150.7$	−126.1	0.4	48.3	8.21

R: Net radiative flux.

Table 6
Heat fluxes at the outside wall (Q_{OW}), glass sheet (Q_{GS}), enthalpy fluxes through the upper (Q_{UV}) and bottom opening vents (Q_{BV}) and volumetric flow rate (G_V) with (NC-R) and without (NC) surface radiation for different external temperatures

T_c [°C]	Q_{OW} [W·m^{-1}]	Q_{GS} [W·m^{-1}]	Q_{UV} [W·m^{-1}]	Q_{BV} [W·m^{-1}]	G_V [m^3·h^{-1}]
−5 NC	166.4	−6.8	−156.4	−2.8	44.2
NC-R	356.1 $R_{OW} = 199.6$	−176.7 $R_{GS} = -197.6$	−191.2	10.7	54.4
5 NC	69.9	−3.4	−62.2	−4.1	35.8
NC-R	167.8 $R_{OW} = 102.8$	−93.1 $R_{GS} = -101.8$	−70.2	−5.0	40.8

R: Net radiative flux.

significant effect is seen along the glass sheet: a boundary flow develops along its surface in contact with the internal ambient, with maximal downward velocities located at about one third of the boundary layer thickness, as for natural convection along an isothermal plate. These maximal velocities have a magnitude of the order of 30% less than the velocities within the enclosure.

- The temperature fields plotted in Fig. 5(b) show that the temperature of the glass sheet is more uniform and that the maximum temperature is less than the internal ambient temperature. This trend is magnified as K_e increases because the radiative cooling increases too.

Surface radiation effects are better exemplified through plots of the vertical temperature distributions along the fluid–solid interfaces at $x = 0$ and $x = D$ drawn in Fig. 6. It should be noted that the horizontal temperature gradient in the glass sheet is almost zero whatever the value of K_e is because its conductive resistance is very low. The radiative cooling of the glass sheet and the large decrease of the vertical temperature gradient is clearly exhibited for all of the cases considered. Returning to the practical application which has motivated the present study, it can be concluded that the use of a protective outside wall made in a single glass sheet is inefficient to prevent condensation of internal humid air on the internal glass sheet (internal ambient at $T_h = 15\,°C$ with a 80% relative humidity). In other words, to have neglected the radiative cooling effect was one of the main reason explaining the reported inefficiencies of many protective glazing of stained-glass windows built so far.

Returning to Fig. 4 (labeled as NC-R), it shows that the main effects of radiation are to produce large decreases in the average temperature of the glass sheet while only quite small increases in the temperature of the facing surface of the outside wall are predicted. Therefore, the effective Rayleigh number is about halved when radiation is taken into account, irrespective of the value of K_e. The heat fluxes reported in Table 5 indicate that net radiative fluxes at the vertical cold and hot facing surfaces are always larger than the natural convection heat fluxes, $(Q_{OW} - R_{OW})$ and $(Q_{GS} - R_{GS})$ respectively, by about 50% at the outside wall and, as much as one order of magnitude larger at the glass sheet. Contrary to what has been found by neglecting radiation (negative sign in the Q_{GS}-values reported in Table 4), the glass sheet is heated by natural convective flows of hot air along its both sides since the $(Q_{GS} - R_{GS})$-values reported in Table 5 are positive.

Therefore, the effect of surface radiation is somewhat more complicated for the vented enclosure considered in the present study than for classical cavity flows. Two driving temperature differences must be indeed accounted for: the difference between the averaged temperatures of the facing surfaces, noted as ΔT_{eff} in Table 5, and the temperature difference between the glass sheet and T_h.

Finally, computations were carried out for two additional external ambient temperature, $T_c = -5\,^{\circ}\mathrm{C}$ and $T_c = +5\,^{\circ}\mathrm{C}$, respectively. For both cases, the conductance of the outside wall was maintained at $K_e = 40.6\ \mathrm{W{\cdot}m^{-2}{\cdot}K^{-1}}$ and the internal ambient temperature at $T_h = 15\,^{\circ}\mathrm{C}$. The results reported in Table 6 add to those already discussed. The main feature which can be drawn is that the surface radiation increasingly contributes to the heating of the outside wall as the temperature difference between internal and external ambiences decreases. These results, not commonly inferred, are supported by the contributions of radiation to Q_{OW}, as shown in Table 6: the contribution by radiation decreases from 61% to 56% as ΔT increases from $10\,^{\circ}\mathrm{C}$ to $20\,^{\circ}\mathrm{C}$. This result can be explained by a 40% increase in the flow rate through the enclosure for a $10\,^{\circ}\mathrm{C}$ increase in ΔT.

5. Conclusions

The salient conclusions from the present study on natural convection-radiation interaction at room temperatures are:

- The temperatures of the outside wall increase when surface radiation is accounted for while the average temperature difference between the two vertical facing walls decreases.
- The radiative contributions to the heat transfer along the facing surfaces were found to be the dominant heat transfer mode for all of the cases considered.
- To neglect radiation in the design of air-vented enclosures with wall temperatures floating to equilibrium distributions between two extreme temperatures leads to highly inaccurate predictions.

Acknowledgements

The authors wish to thank the IDRIS-Computer Center (French National Institute for Advances in Scientific Computations) for the computational support through Grant No. 04-1265.

References

[1] D.M. Sefcik, B.W. Webb, H.S. Heaton, Natural convection in vertically vented enclosures, Trans. ASME J. Heat Transfer 113 (1991) 912–918.
[2] G. Desrayaud, G. Lauriat, A numerical study of natural convection in partially open enclosures with a conducting side-wall, Trans. ASME J. Heat Transfer 126 (2004) 76–83.
[3] G. Lauriat, Combined radiation–convection in gray fluids enclosed in vertical cavities, Trans. ASME J. Heat Transfer 104 (1982) 609–615.
[4] G. Lauriat, Numerical study of the interaction of natural convection with radiation in non-grey gases in a narrow vertical cavity, in: Proc. 7th Int. Heat Transfer Conf., Munich, vol. 2, 1982, pp. 153–158.
[5] L.C. Chang, K.T. Yang, J.R. Lloyd, Radiation-natural convection interaction in two-dimensional complex enclosures, Trans. ASME J. Heat Transfer 105 (1983) 89–95.
[6] G. Desrayaud, G. Lauriat, Radiative influence on the stability of fluids enclosed in vertical cavities, Internat. J. Heat Mass Transfer 31 (5) (1988) 1035–1048.
[7] T. Fusegi, B. Farouk, Laminar and turbulent natural convection–radiation interaction in a square enclosure filled with a nongray gas, Numer. Heat Transfer A 15 (1989) 303–322.
[8] G. Lauriat, A numerical study of a thermal insulation enclosure: influence of the radiative transfer, Natural Convection in Enclosures, ASME-HTD 8 (1980) 63–71.
[9] H. Nakamura, Y. Asako, H. Hirat, Combined free convection and radiation heat transfer in rectangular cavities with a partition wall, Heat Transfer Japan. Res. (1986) 60–81.
[10] J.L. Lage, J.S. Lim, A. Bejan, Natural convection with radiation in a cavity with open top end, Trans. ASME J. Heat Transfer 114 (1992) 479–486.
[11] C. Balaji, S.P. Venkateshan, Interaction of surface radiation with free convection in a square cavity, Internat. J. Heat Fluid Flow 14 (1993) 260–267.
[12] C.Y. Han, S.W. Baek, The effects of radiation on natural convection in a rectangular enclosure divided in two partitions, Numer. Heat Transfer A 37 (1989) 303–322.
[13] A. Akiyama, Q.P. Chong, Numerical analysis of natural convection with surface radiation in a square enclosure, Numer. Heat Transfer A 32 (1997) 419–433.
[14] N. Ramesh, W. Merzkirch, Combined convective and radiative heat transfer in side-vented open cavities, Internat. J. Heat Fluid Flow 22 (2001) 180–187.
[15] S.N. Sing, S.P. Venkateshan, Numerical study of natural convection with surface radiation in side vented open cavities, Internat. J. Therm. Sci. 43 (2004) 865–876.
[16] S.N. Sing, S.P. Venkateshan, Natural convection with surface radiation in partially open cavities, Internat. J. Heat Technol. 23 (2) (2004) 55–62.
[17] H. Wang, S. Xin, P. Le Quéré, Étude numérique du couplage de la convection naturelle avec le rayonnement de surfaces en cavité carrée remplie d'air, C. R. Acad. Sci. Mécanique 334 (1) (2006) 48–57.
[18] J. Salat, Contribution à l'étude de la convection naturelle en cavité différentiellement chauffée, PhD thesis, Univ. Poitiers, 2004.
[19] A.H. Abib, Y. Jaluria, Numerical simulation of buoyancy induced flow in a partially open enclosure, Numer. Heat Transfer A 14 (1988) 235–254.
[20] E.M. Sparrow, R.D. Cess, Radiation Heat Transfer, Hemisphere, Washington, DC, 1978.
[21] K.A.R. Ismail, J.R. Henriquez, Two-dimensional model for the double glass naturally ventilated window, Internat. J. Heat Mass Transfer 48 (2005) 461–475.
[22] S. Oidtmann, H. Schellen, Shutzverglasung vor historischen glasgemälden—eine theoretische betrachtung, Bauphysik 14 (1992) 138–145.
[23] ASHRAE, Handbook of Fundamentals, American Society of Heating, Refrigerating and Air-Conditioning Engineers, USA, 1993, Chapter 27: Fenestration.
[24] E.M. Sparrow, L.F.A. Azevedo, Vertical-channel natural convection spanning between the fully-developed limit and the single-plate boundary-layer limit, Internat. J. Heat Mass Transfer 28 (1985) 1847–1857.